Preparation and heterogeneous photocatalytic activity of mesoporous $H_3PW_{12}O_{40}/ZrO_2$ composites

Xuesong Qu [a], Yihang Guo [a,*], Changwen Hu [b,**]

[a] *Faculty of Chemistry, Northeast Normal University, Changchun 130024, PR China*
[b] *Department of Chemistry, Beijing Institute of Technology, Beijing 100081, PR China*

Available online 22 August 2006

Abstract

A series of mesoporous zirconia supported Keggin units with different $H_3PW_{12}O_{40}$ loading levels (5–20 wt.%) and phase structures (amorphous, tetragonal, and the mixed phases of tetragonal and monoclinic) are prepared by a modified wet impregnation method. The phase structures, chemical structures, optical absorption properties, surface physicochemical properties, and morphologies of the composites are well-characterized via X-ray diffraction (XRD) patterns, FT-IR spectroscopy, Raman scattering spectroscopy, UV–vis diffuse reflectance spectroscopy (UV–vis/DRS), nitrogen adsorption/desorption determination, and field emission scanning electron microscopy (FESEM), indicating that the primary Keggin structure remained intact after formation of the composites, and impregnation of the Keggin unit into the surface of ZrO_2 framework has an influence on the electronic properties of the ZrO_2. The heterogeneous photocatalytic activity of as-prepared composites is studied via the model reactions of degradation of an aqueous 4-nitrophenol (4-NP) and dye methylene blue (MB) under aerobic condition, indicating that the photocatalytic activity of the composites was influenced by the factors such as phase structures, optical absorption properties, and surface physicochemical properties of the composites.
© 2006 Elsevier B.V. All rights reserved.

Keywords: Composites; Photocatalytic activity; Wet impregnation; Physicochemical properties

1. Introduction

Heterogeneous photocatalysis by solid polyoxometalate (POM) is a new branch in the field of photocatalytic chemistry, and some attractive researching progresses have developed in recent years. Although POMs exhibit UV-light photocatalytic activity in homogeneous system, the main disadvantages of them as photocatalysts lie in their low surface area and difficulty of separation from the reaction mixture. Therefore, development of novel solid catalysts with advanced characteristics such as surface area and porosity has been a challenge for a long time. Recent studies showed that immobilization of soluble POM units with different structures into the suitable supports (*i.e.*, silica, mesoporous molecular sieve MCM-41 or MCM-48, NaY zeolite, activated carbons, layered double hydroxide, amorphous or anatase TiO_2) are an effective method to overcome the mentioned problems [1–12].

In this paper, a series of novel solid Keggin-type POMs are prepared by using ZrO_2 as the support. ZrO_2 is an important material widely used in ceramics technology [13] and in heterogeneous catalysis [14,15]. In the field of catalysis, ZrO_2 can be served as a catalyst or catalyst support. In addition, as the same as TiO_2, ZrO_2 is an n-type semiconductor oxide that has also been tested for performing photocatalytic reactions [16,17]. The photocatalytic activity of ZrO_2 has been successfully tested although it has been well established that the photoactivity per unit surface area is far less than that shown by TiO_2 [16]. This is due to high band gap energy of ZrO_2 (5.0 eV corresponding to an absorption edge to close to 250 nm [18]). It is expected that impregnation of photoactive Keggin unit into the surface of ZrO_2 framework can improve its photocatalytic activity. So far, the results concerning about addition of POM (mainly Keggin unit) on the stabilized or hydrated ZrO_2 support has been reported [19,20], and their acid-catalyzed property has been investigated. The studies pointed out that the chemical interactions between the Keggin unit and the ZrO_2 support are a matter of great interest because a strong interaction could fix the Keggin unit into the carrier, avoiding the leaching of the Keggin unit in liquid-phase reactions [21,22]. Here, the $H_3PW_{12}O_{40}/ZrO_2$

---

* Corresponding author. Tel.: +86 431 5099762; fax: +86 431 5099762.
** Corresponding author. Tel.: +86 10 62828869; fax: +86 10 62828869.
E-mail addresses: guoyh@nenu.edu.cn (Y. Guo), cwhu@bit.edu.cn (C. Hu).

composites with different $H_3PW_{12}O_{40}$ doping levels and phase structures are prepared by a modified wet impregnation method. Considering the thermal stability of $H_3PW_{12}O_{40}$ and avoiding its decomposition during the calcination process, ZrO_2 (rather than $H_3PW_{12}O_{40}/ZrO_2$) supports with different phase structures are firstly prepared via calcination of the hydrous ZrO_2 at different temperatures. The $H_3PW_{12}O_{40}/ZrO_2$ composites are produced by incorporation of the $H_3PW_{12}O_{40}$ unit into the different ZrO_2 supports. The phase structures, chemical structures, optical absorption properties, surface physicochemical properties, and morphologies of the $H_3PW_{12}O_{40}/ZrO_2$ composites are well-characterized via XRD patterns, FT-IR spectroscopy, Raman scattering spectroscopy, UV–vis/DRS, nitrogen adsorption/desorption determination, and FESEM. The heterogeneous photocatalytic activity of as-prepared composites with different phase structures is studied systematically via the model reactions of UV-light photodegradation of an aqueous 4-NP and MB.

Purpose of this study is to develop novel supported POM photocatalytic materials, for example, ZrO_2-supported Keggin unit with different phase structures (amorphous, tetragonal, and the mixture of tetragonal and monoclinic). The photocatalytic activity of as-prepared materials is evaluated afterwards, and the relationships between the heterogeneous photocatalytic activity and their phase structures, optical absorption properties, surface physicochemical properties, or $H_3PW_{12}O_{40}$ doping levels are studied.

2. Experimental

2.1. Catalyst preparation

Zirconia supports with different phase structures are prepared by sol–gel method, and the process is described below. The mixture of zirconium n-butoxide ($Zr(n\text{-}OC_4H_9)_4$, 21 mmol) and ethanol (870 mmol) is stirred vigorously for 1 h at room temperature. In addition, water (84 mmol) and HCl (2 mmol) are added dropwise into the above $Zr(n\text{-}OC_4H_9)_4$ solution, respectively. The resulting mixture is stirred until the transparent $Zr(OH)_4$ sol is obtained. After aging for 12 h, the gel particulate is dried in air at 373 K for 24 h. Eventually, the product is calcined at different temperatures (623, 773, and 923 K, respectively) for 3 h.

The $H_3PW_{12}O_{40}/ZrO_2$ composites are prepared by a modified wet impregnation method, and the process is described below. Zirconia support (1 g) was suspended in the different amounts of ethanol solution containing 2.5 mmol of $H_3PW_{12}O_{40}$ in order to obtain a series of catalysts with different $H_3PW_{12}O_{40}$ loading levels (i.e., 5, 10, 15, 20 wt.%). The above suspension is stirred at room temperature for 12 h while reflux is used. Ethanol is removed at 353 K. The product is dried at 373 K for 2 h, and then it is washed for three times with hot water. The final product is obtained by drying at 333 K for 24 h in air. Before the photocatalytic test, the product is calcined at 473 K in a vacuum oven for 2 h. As-prepared catalysts are represented by xTZ-t, where x refers to weight percentage of $H_3PW_{12}O_{40}$ (wt.%), T $H_3PW_{12}O_{40}$, Z zirconia, and t refers to calcination temperature (K) of preparation of the ZrO_2 support.

Table 1
$H_3PW_{12}O_{40}$ loading level and characteristic IR absorption peaks of the $H_3PW_{12}O_{40}$ in the $H_3PW_{12}O_{40}/ZrO_2$ composites

| Catalyst	$H_3PW_{12}O_{40}$ loading level (%)	Wavenumber (cm^{-1})			
		P(Zr)-O_a	W=O_d	W–O–W	W–O–W
5 TZ-623	4.62	1069.2	979.2	874.9	798.1
10 TZ-623	9.10	1086.7	978.6	871.9	794.7
15 TZ-623	14.12	1081.3	967.4	883.9	786.8
20 TZ-623	18.3	1089.4	955.1	900.7	798.0
5 TZ-773	3.91	1083.1	976.2	879.4	796.2
10 TZ-773	8.04	1085.6	974.3	878.6	795.4
15 TZ-773	13.56	1084.5	973.5	876.8	796.3
20 TZ-773	17.8	1083.8	969.1	873.1	794.1
5 TZ-923	3.25	1080.4	980.9	879.2	798.6
10 TZ-923	6.87	1082.3	978.7	875.9	797.9
15 TZ-923	9.57	1081.7	976.8	876.0	792.7
20 TZ-923	10.85	1080.1	979.1	873.8	790.4
ZrO_2-623	–[a]	1103.8	–[a]	–[a]	–[a]
$H_3PW_{12}O_{40}$	100	1080.0	988.2	894.6	811.9

[a] Not found.

2.2. Characterization

The loading levels of the $H_3PW_{12}O_{40}$ in the final composites are determined by a Leeman Prodigy inductively coupled plasma atomic emission spectrometer (ICP-AES), and the results are summarized in Table 1. XRD patterns of the samples (pure powders) are obtained with a Rigaku D/max-3c X-Ray diffractometer with Cu Kα radiation. UV–vis/DRS (pure sample powder mixing with $BaSO_4$ powder) are recorded on a Cary 500 UV–VIS-NIR spectrophotometer. FI-IR spectra are taken in a Nicolet magna 560 IR spectrophotometer. FESEM images are obtained on a XL-30 ESEM FEG scanning electron microscope, and the samples are dispersed into absolute ethanol firstly. Raman spectra are recorded on a Jobin-Yvon HR 800 instrument with an Ar^+ laser source of 488 nm wavelengths in a macroscopic configuration. BET specific surface area and BJH pore size are calculated from nitrogen adsorption/desorption isotherms determined at $-196\,°C$ using an ASAP 2010 M surface analyzer (the samples were outgassed under vacuum at $200\,°C$).

2.3. Photocatalytic testing

The photoreactor is designed with a cylindrical quartz cell configuration and an internal light source surrounded by a quartz jacket where the suspension of catalyst and aqueous organics completely surrounded the light source. An external cooling flow of water was used to maintain the temperature of the system at $30 \pm 2\,°C$. UV-light energy is provided by a 50 W high pressure mercury lamp (HPML).

The photocatalytic activity of as-prepared catalysts is tested by the model reactions of photodecomposition of an aqueous 4-NP and dye MB (its structure is shown in Scheme 1). In a typical reaction, the solid catalyst (0.1 g) is suspended in an aqueous solution of 4-NP ($C_o = 0.36\,mmol\,l^{-1}$, 100 ml) or MB ($C_o = 0.065\,mmol\,l^{-1}$, 100 ml), and then ultrasonicate for 10 min to make the catalyst homogeneously disperses into the reaction solution. Before UV-light irradiation, the suspen-
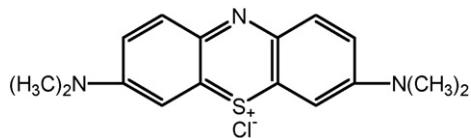
Scheme 1. Structure of methylene blue (MB).

sion is stirred in the dark for 30 min to ensure establishment of adsorption–desorption equilibrium. The suspension is vigorously stirred and the system opens to air during the whole process. The concentration of 4-NP is monitored by a Shimadzu LC-8A high-pressure liquid chromatography (HPLC) using UV detector at 210 nm. The concentration of MB is analyzed by a Cary 500 UV–VIS-NIR spectrophotometer at $\lambda_{max} = 664$ nm. Before determination, the withdrawn suspensions are centrifuged and filtered with the microporous membrane.

3. Results and discussion

3.1. Catalyst preparation and characterizations

Hydrous zirconia support is prepared by a sol–gel method via hydrolysis of the $Zr(n\text{-}OC_4H_9)_4$ under acidic condition. After calcination of the resulting hydrous ZrO_2 at 373, 623, 773, and 923 K, respectively, zirconia with amorphous, tetragonal, and the mixture of tetragonal and monoclinic phases are produced (Fig. 1). Impregnation of the Keggin unit into zirconia support is obtained via suspending the support into the $H_3PW_{12}O_{40}$–ethanol solution. During this process, $H_3PW_{12}O_{40}/ZrO_2$ composites are formed via electrostatic interactions and hydrogen bonding. The hydrogen bonding are formed in the composites between the oxygen atoms of the Keggin anion and the surface hydroxyl groups of the zirconia network ($\equiv Zr\text{-}OH$), which can be expressed in the forms of $W=O_t\cdots HO\text{-}Zr\equiv$, $W\text{-}O_c\cdots HO\text{-}Zr\equiv$, and $W\text{-}O_e\cdots HO\text{-}Zr\equiv$, where O_t and O_c or O_e refers to the terminal oxygen atoms and the bridge oxygen atoms, respectively, in the Keggin unit [23,24]. These two interactions would ensure to fix the $H_3PW_{12}O_{40}$ unit into the ZrO_2 support firmly, so that the leaching of $H_3PW_{12}O_{40}$ in liquid phase reactions may be avoided.

3.1.1. XRD patterns

Phase structures of ZrO_2 supports obtained by calcination of hydrous ZrO_2 at different temperatures and their corresponding $H_3PW_{12}O_{40}/ZrO_2$ composites are analyzed by XRD (Fig. 1). Both the ZrO_2 support obtained via calcination at 373 K (ZrO_2-373) and its corresponding $H_3PW_{12}O_{40}/ZrO_2$ composite (15 TZ-373) are in the amorphous phase. Increase the calcination temperature to 623 K, both the ZrO_2 support (ZrO_2-623) and its corresponding $H_3PW_{12}O_{40}/ZrO_2$ composite (5 TZ-623) are mainly in the tetragonal phase with the characteristic 2θ values at 30.1° (1 1 1), 35.2° (2 0 0), 50.4° (2 2 0), and 59.9° (3 1 1), respectively (Fig. 1a, JCPDS file 17-0923). Continuous increasing the calcination temperature to 773 K, the mixed tetragonal and monoclinic phases are formed for both ZrO_2
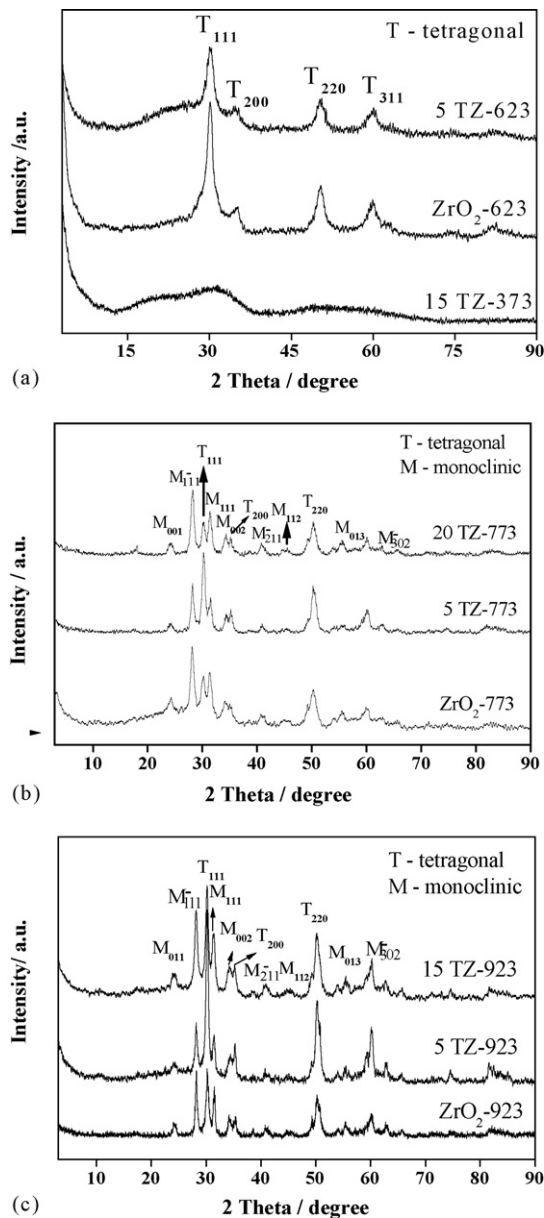

Fig. 1. XRD patterns of the ZrO_2 support and $H_3PW_{12}O_{40}/ZrO_2$ composites with different calcination temperatures.

support and the corresponding $H_3PW_{12}O_{40}/ZrO_2$ composites (ZrO_2-773, 20 TZ-773, and 5 TZ-773, Fig. 1b). The new diffraction peaks locate at 24.0° (0 1 1), 28.2° ($\bar{1}$ 1 1), 31.4° (1 1 1), 34.3° (0 0 2), 40.7° ($\bar{2}$ 1 1), 44.5° (1 1 2), 55.5° (0 1 3), and 60.1° ($\bar{3}$ 0 2), respectively, corresponds to the diffractions of monoclinic ZrO_2 phase (JCPDS file 86-1450). As the ZrO_2 support is calcined to 923 K, the mixed tetragonal and monoclinic phases are also formed. The crystallinity of the composites (5 TZ-923 and 15 TZ-923) increases compared with the TZ-773 samples (Fig. 1c). In addition, no indication of any crystalline phase related to $H_3PW_{12}O_{40}$ appears even though the loading level of the $H_3PW_{12}O_{40}$ reaches to 20 wt.%. This result implies that the Keggin unit homogeneously disperses into the surface of ZO_2 framework, which will be benefit to enhance the catalytic activity of the composites. On the other
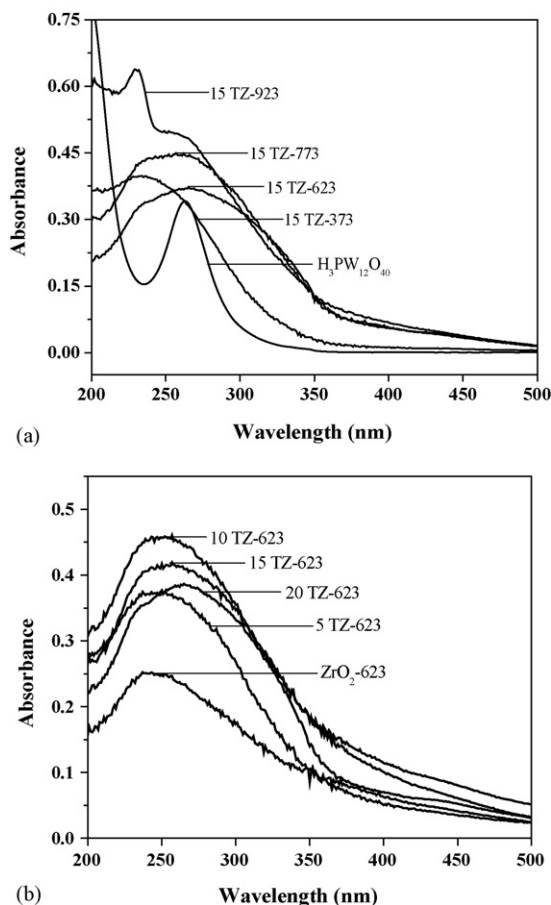
Fig. 2. (a) UV/DR spectra of 15 TZ-t composites with the different ZrO_2 calcination temperature, where $t = 373, 623, 773$, and 923 K, respectively. (b) UV/DR spectra of the xTZ-623 composites with different $H_3PW_{12}O_{40}$ doping levels, where $x = 5, 10, 15$, and 20, respectively.

hand, it can infer that different $H_3PW_{12}O_{40}$ loading levels have little effect on the ZrO_2 phase structures.

3.1.2. Optical absorption properties

The optical absorption properties of the ZrO_2 supports and the corresponding $H_3PW_{12}O_{40}/ZrO_2$ composites are studied by UV–vis/DR spectroscopy (Fig. 2). At first, with the same $H_3PW_{12}O_{40}$ doping level (15 wt.%) but different phase structures, the electronic spectra of the $H_3PW_{12}O_{40}/ZrO_2$ are obviously different (Fig. 2a). That is, O 2p to W 5d charge transfer (CT) bands of the starting $H_3PW_{12}O_{40}$ appear at $ca.$ 200 (W=O_t bond) and 260 nm (W–$O_{c/e}$–W bond), respectively. O 2p to Zr 4d CT band of ZrO_2-623 appears at 237 nm. After formation of the crystalline $H_3PW_{12}O_{40}/ZrO_2$ composites (*i.e.*, 15 TZ-623 and 20 TZ-773), the original O 2p to W 5d or O 2p to Zr 4d CT bands disappear, whereas, a broad absorption peak appear with the red shift of the CT band compared with ZrO_2 support or the starting Keggin unit. However, as for the 15 TZ-923, two solitary absorption peaks corresponding to O 2p to W 5d and O 2p to Zr 4d charge transfer appear again. This is due to the surface properties of the ZrO_2 support. When the ZrO_2 support is calcined at 923 K, both the amount of hydroxyl groups of the ZrO_2 and its specific surface area decreased, accordingly, $H_3PW_{12}O_{40}$ tends

to saturate in the composite after $H_3PW_{12}O_{40}$ loading level is up to $ca.$ 10 wt.%. With the increase of the $H_3PW_{12}O_{40}$ loading level, the excessive $H_3PW_{12}O_{40}$ physically adsorbs on the surface of the catalyst, at least partially, resulting in partial segregation of the Keggin unit from the ZrO_2 support. As for the 15 TZ-373, its OMCT (233 nm) band is shorter than that of 15 TZ-623 or 20 TZ-773, suggesting that the different phase structures have an effect on their optical absorption properties. By using the same ZrO_2 support (ZrO_2-623) but different $H_3PW_{12}O_{40}$ doping levels, the positions and shapes of the OMCT bands are very similar, implying that different $H_3PW_{12}O_{40}$ doping levels have little effect on the optical absorption properties of the composites (Fig. 2b).

The above UV–vis/DRS results indicate that impregnation of the Keggin unit into the ZrO_2 framework (ZrO_2-623 and ZrO_2-773) had an influence on the electronic properties of the ZrO_2, resulting in red shift of the OMCT band. This is due to formation of a doping energy level (or moderate widening of electronic band) between the conduction (Zr 4d) and valence bands (O 2p) of ZrO_2. The electronic transitions from the valence band (O 2p) to dopant level or from the dopant level to the conduction band (W 5d + Zr 4d) can effectively red shift the band edge absorption threshold. This optical absorption property will be beneficial to improve the photocatalytic activity of ZrO_2 since the transition from the valence band to the dopant level or from the dopant level to the conduction band become easier, resulting in more photogenerated electrons (e^-) and holes (h^+) to participate the photocatalytic reactions. In addition, the band gap of the crystalline ZrO_2 is narrower than that of the amorphous one.

3.1.3. FT-IR and Raman scattering spectroscopies

The integrity of the Keggin structure in as-prepared composites is confirmed by FT-IR (Table 1 and Fig. 3) and Raman scattering spectroscopies (Fig. 4). That is, the composites exhibited four characteristic IR absorption peaks in the range from 700 to 1100 cm^{-1}, corresponding to the stretching vibrations of P–O, W=O, and W–$O_{c/e}$–W bonds of the Keggin unit, respectively [25]. Specifically, the peak appears at $ca.$1080 cm^{-1} is originated from the vibration of P–O bonds, the peak appears
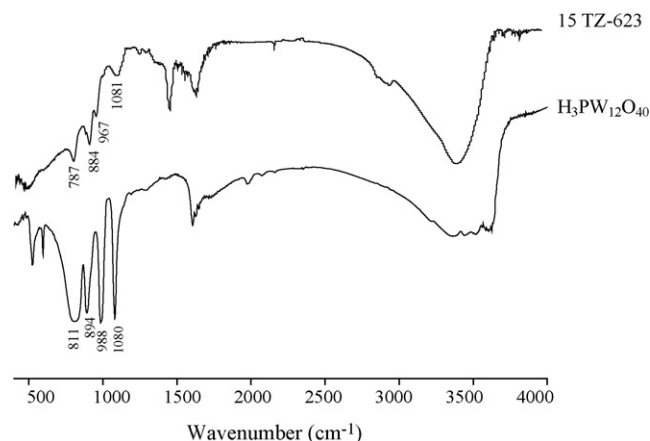

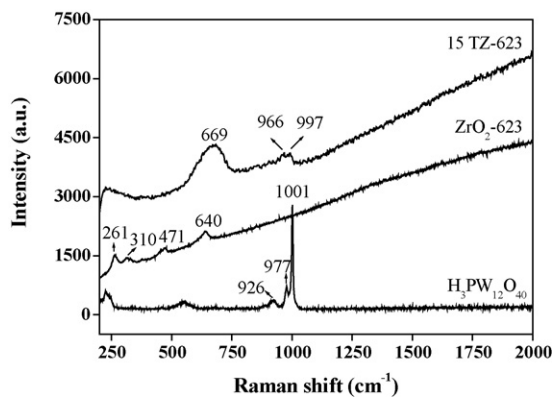Fig. 3. FT-IR spectra of the starting $H_3PW_{12}O_{40}$ and 15 TZ-623.

Fig. 4. Raman scattering spectra of $H_3PW_{12}O_{40}$, ZrO_2-623, and 15 TZ-623.

at *ca.* 980 cm^{-1} corresponds to the vibrations of W=O bonds, and two peaks appear at *ca.* 880 and 800 cm^{-1} were due to the vibrations of the two types of W–O$_{c/e}$–W bridge bonds. Compared with the parent Keggin unit, both shifts of the IR peak positions and broadening of the peak shapes are ascribed to the interactions between the Keggin unit and the ZrO_2 support.

Raman scattering studies further support the above result. That is, three Raman scattering peaks appear at 1001, 977, and, 926 cm^{-1} are observed in the starting $H_3PW_{12}O_{40}$ unit, corresponding to stretching vibrations of P–O bond of the PO$_4$ sites, W=O$_t$ and W–O$_{c/e}$–W bonds, respectively [8]. As for the $H_3PW_{12}O_{40}$/ZrO_2 composites, only two Raman scattering peaks at 997 and 966 cm^{-1} are detected, and their peak intensities decrease compared with those of the starting $H_3PW_{12}O_{40}$. The similar results have been reported by López-Salinas [26]. The red shift of the peak positions and weakening of the peak intensity in comparison with the starting Keggin unit may be due to formation of some W–O–Zr bond on the surface of ZrO_2 support [27]. This weakening of the W=O$_t$ bond may also due to hydrogen bonding between the W=O$_t$ bonds and surface Zr–OH groups. The peak corresponding to W–O$_{c/e}$–W bond disappears in the $H_3PW_{12}O_{40}$/ZrO_2 composite, and the reason is unclear in current study. In addition, the weak peaks located at 200–700 cm^{-1} are the characteristic of tetragonal phase of zirconia, originating from the vibrations of Zr–O or Zr–O–Zr bonds [26].

3.1.4. Surface physicochemical properties

The surface physicochemical properties of as-prepared ZrO_2 and corresponding $H_3PW_{12}O_{40}$/ZrO_2 composites are characterized by N_2 adsorption/desorption analyses, and the representative N_2 adsorption/desorption isotherms and BJH pore size distribution curves are shown in Fig. 5. The calculated BET specific surface area, pore size, and pore volume are summarized in Table 2. The ZrO_2 support calcined at 623 K (ZrO_2-623) exhibits typical mesoporosity according to IUPAC definition, and its isotherm is type IV with the hysteresis loop appearing at an intermediate relative pressure ($p/p_0 = 0.4$ to 0.6, Fig. 5a). After grafting the Keggin unit into the surface of ZrO_2 framework, the isotherm still is type IV with the hysteresis loop showing at
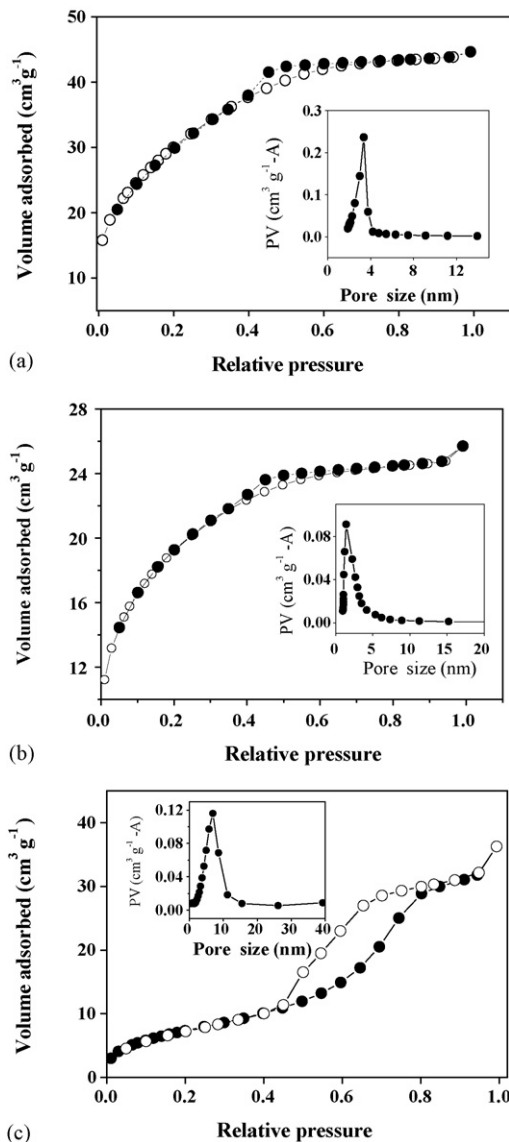

Fig. 5. N_2 adsorption/desorption isotherms and pore size distribution curves (insert) of as-prepared catalysts. (a) ZrO_2-623 K, (b) 15 TZ-623 K and (c) 20 TZ-773 K.

$p/p_0 = 0.4$–0.6 (Fig. 5b). However, the BET surface area, pore diameter, and pore volume decrease, respectively, compared with the ZrO_2 support. As for the 20 TZ-773, its BET surface area further decrease, at the same time, the volume adsorbed

Table 2
Textural properties of the ZrO_2 supports and corresponding $H_3PW_{12}O_{40}$/ZrO_2 composites

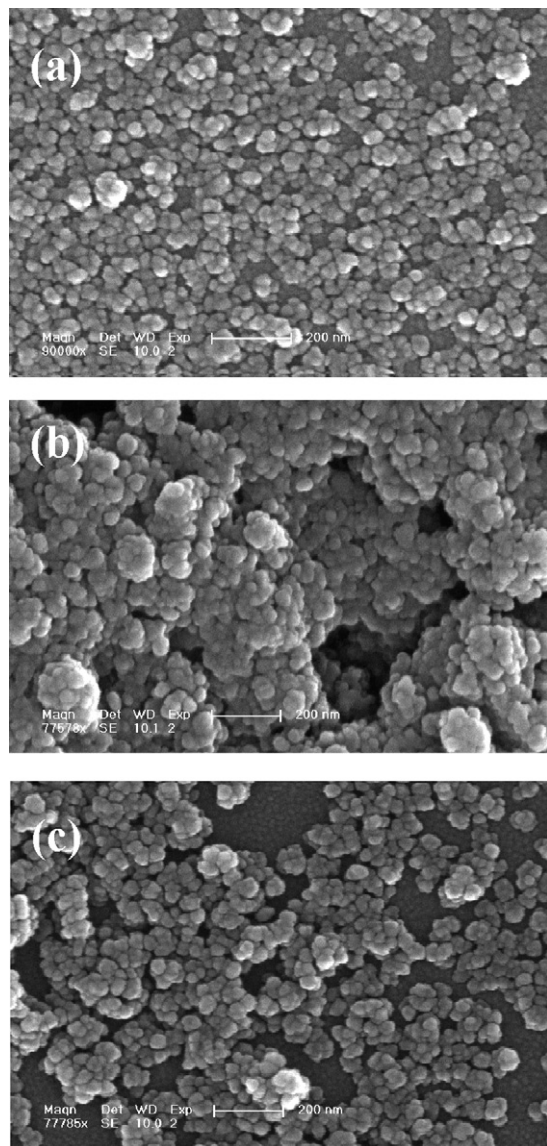| Sample	SA[a] (m^2 g^{-1})	PD[b] (nm)	PV[c] (cm^3 g^{-1})
ZrO_2-623	111.6	3.4	0.26
15 TZ-623	69.4	2.0	0.09
ZrO_2-773	54.3	8.2	0.29
20 TZ-773	39.4	6.9	0.11
ZrO_2-923	29.8	8.6	0.12
10 TZ-923	21.0	6.2	0.08

[a] BET surface area.
[b] Average pore diameter.
[c] Pore volume.

Fig. 6. FESEM images of the $H_3PW_{12}O_{40}/ZrO_2$ composites. (a) 15 TZ-623 K, (b) 15 TZ-773 K, and (c) 15 TZ-923 K.

Fig. 7. Photodegradation of an aqueous 4-NP (0.36 mmol l^{-1}, 100 ml) by UV-light irradiation of ZrO_2 (0.1 g) with different phase structures.

decrease obviously. However, the isotherm of 20 TZ-773 is still type IV with the hysteresis loop showing at $p/p_0 = 0.4$–0.8 (Fig. 5c). The above results indicate that the BET surface areas of the $H_3PW_{12}O_{40}/ZrO_2$ composites are lower than that of the ZrO_2 support. This is due to the preparation method used here. After grafting the large Keggin unit on the surface of the ZrO_2 support, some of the pores of ZrO_2 are blocked up with the decrease of its BET surface area and pore volume. In addition, with the increase of the calcination temperature, the BET surface area of the corresponding composites decreases owing to the crystallinity of the product being increased.

3.1.5. Morphology

FESEM images of the composites are shown in Fig. 6. It is observed that the particles are spherical and exhibited uniform distribution with an average size of 25–30 nm, at the same time, aggregation among particles occurred.
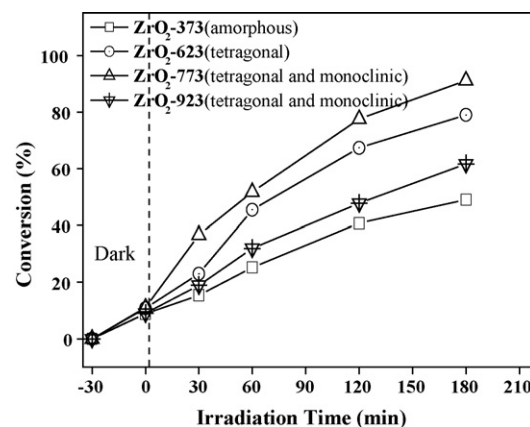
3.2. Photocatalytic testing

3.2.1. UV-light photocatalytic activity of the ZrO_2 supports

It is well known that the photoactivity of the catalyst is influenced by its crystal phase structures. For example, the photoactivity of TiO_2 in the anatase phase is higher than that of other phases. However, little work has been done on studies of the photocatalytic behavior of the ZrO_2 in the different phase structures. Here, 4-NP is chosen as one of the model reactant to investigate the relationships between the heterogeneous photocatalytic activity and the ZrO_2 phase structures. 4-NP is an intermediate product that involves in the process of degradation of pesticides and hardly removal because of its high stability. Photodegradation of an aqueous 4-NP ($C_o = 0.36$ mmol l^{-1}, 100 ml) in the absence of the photocatalyst is neglectable because there is no any change of its concentration after 4 h UV-light irradiation. Fig. 7 shows change of 4-NP conversion under UV-light irradiation of the different ZrO_2 supports. It can be clearly seen that the concentration of the 4-NP decreases in some extents by using different ZrO_2 supports. ZrO_2-773 exhibits the highest photocatalytic activity, while ZrO_2-373 exhibits the lowest photocatalytic activity among the four tested ZrO_2 supports. The above results indicate that the four ZrO_2 supports are photoactive, and the crystalline ZrO_2 are more photoactive than that of the amorphous one. As for the ZrO_2-923, it has the similar phase structure with that of the ZrO_2-773, however, its photocatalytic activity is relatively low. The reason may be due to its lower BET surface area. In subsequent studies, only ZrO_2-773 is selected as the support of $H_3PW_{12}O_{40}$.

3.2.2. UV-light photocatalytic activity of the $H_3PW_{12}O_{40}/ZrO_2$ composites

For the sake of enhancement of the photocatalytic activity of ZrO_2 and $H_3PW_{12}O_{40}$, the TZ-773 composites with different $H_3PW_{12}O_{40}$ doping levels are prepared, and their photocatalytic activity is evaluated by degradation of aqueous 4-NP (Fig. 8) and MB (Fig. 9). Homogeneous $H_3PW_{12}O_{40}$ and zirconia support are also tested for comparison under the same conditions. Homogeneous $H_3PW_{12}O_{40}$ exhibits low photocatalytic activity to 4-NP degradation, however, obvious 4-NP

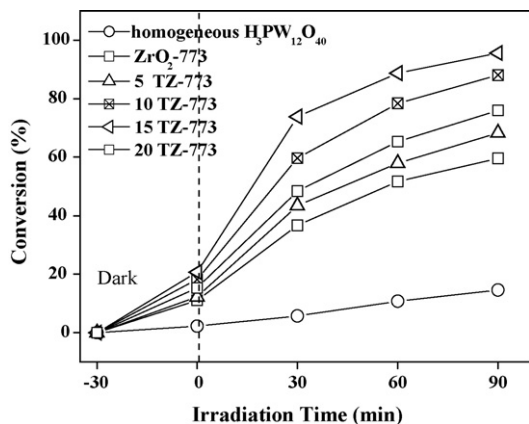Fig. 8. Photodegradation of an aqueous 4-NP ($0.36\,\mathrm{mmol\,l^{-1}}$, 100 ml) by UV-light irradiation of the different $H_3PW_{12}O_{40}/ZrO_2$ composites (0.1 g).

degradation is observed by using the $H_3PW_{12}O_{40}/ZrO_2$ as the photocatalysts. Moreover, the photocatalytic activity improves with increasing $H_3PW_{12}O_{40}$ loading levels from 5 to 15 wt.%. However, once the $H_3PW_{12}O_{40}$ loading level is up to 20 wt.%, the photocatalytic activity decreases obviously. This may be due to the fact that the Keggin unit homogeneously disperses into the framework of ZrO_2 if the $H_3PW_{12}O_{40}$ loading levels are less than 15 wt.% [28,29]. This homogeneous dispersion of the Keggin unit into the ZrO_2 framework plays important role to improve the photocatalytic activity of the composites. When the $H_3PW_{12}O_{40}$ loading level is higher than 20%, partial segregation of the Keggin unit from the ZrO_2 support occurs, accordingly, the photocatalytic activity decreases.

In order to further test the photocatalytic activity of as-prepared composites, MB is selected as another model reactant. MB is a heteropolyaromatic dye with large and complicated structure (Scheme 1) that is difficult to be degraded. All the experimental conditions used are same with those of 4-NP degradations. Fig. 9 shows change of MB conversion by UV-light irradiating the suspension including an aqueous MB ($0.065\,\mathrm{mmol\,l^{-1}}$, 100 ml) and the TZ-773 composites (0.1 g) with different $H_3PW_{12}O_{40}$ loading levels. MB direct photolysis results shows that disappearance of MB is negligible. In addi-
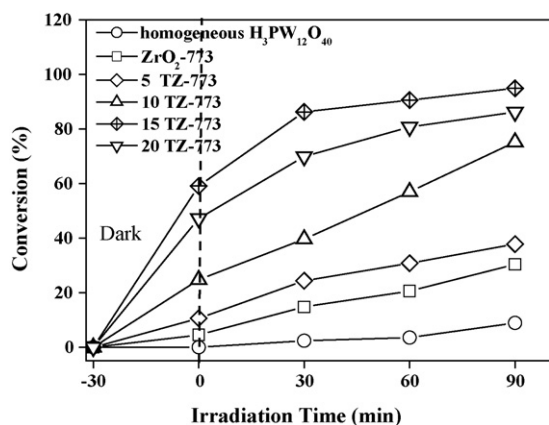
tion, the photocatalytic activity of the starting $H_3PW_{12}O_{40}$ or ZrO_2-773 was low to MB degradation. However, significant MB degradation is observed by UV-light irradiation of the TZ-773 composites, and the 15 TZ-773 exhibits the highest photocatalytic activity among the six tested photocatalytic materials. The above results are in agreement with those of the 4-NP degradation, further confirming the enhanced photocatalytic activity by impregnation of the Keggin unit into the ZrO_2 support.

It must be emphasized that the concentration of 4-NP or MB has decreased before UV-light irradiation, indicating that adsorption of the ZrO_2 or $H_3PW_{12}O_{40}/ZrO_2$ to the 4-NP or MB molecule occurred. This adsorption results in more easily degradation of the 4-NP or MB molecules. In a heterogeneous photocatalysis system, photo-induced molecular transformations or reactions take place at the surface of a catalyst, and the adsorption of the reactant molecules on the surface of the catalyst is the first step of photocatalytic reaction [30]. Difference of adsorption ability between the ZrO_2 and $H_3PW_{12}O_{40}/ZrO_2$ may be explained below. The hydroxyl group of the zirconia can't be protonated or deprotonated at pH 6–7 [31], therefore, 4-NP or MB is difficult to be adsorbed on the surface of the ZrO_2. In the case of the $H_3PW_{12}O_{40}/ZrO_2$ composites, 4-NP or MB molecule may adsorbed on their surface by hydrogen bonds formed between the catalyst and the reactant molecules, which may be an essential premise for the photocatalytic degradation of 4-NP or MB.

On the basis of the above experimental results and the characteristics of as-prepared $H_3PW_{12}O_{40}/ZrO_2$ composites in phase structures, surface physicochemical properties, and electronic attributes, we infer that the following two factors could contribute to this increased photocatalytic efficiency compared with that of the ZrO_2 or $H_3PW_{12}O_{40}$. On the one hand, relatively narrow band gap of the composites and increase the amount of photochemistry at longer wavelengths play an important role to this enhanced photocatalytic activity. Therefore, electron transition from the valence band to the dopant level or from the dopant level to the conduction band become easier, resulting in more photogenerated electrons (e^-) and holes (h^+) to participate the photocatalytic reactions. Higher photocatalytic activity of the crystalline ZrO_2 than that of the amorphous ZrO_2 is also due to this fact. On the other hand, the surface physicochemical properties of the mesoporous materials also play significant role to this enhanced photocatalytic activity. Compared with the starting POM, as-prepared composites show relatively high BET surface area. Therefore, more contact areas between the catalyst and the substrate are provided for the surface-mediated electron-transfer reactions to take place. In addition, the porous catalysts show a strong adsorption to the substrates, which is beneficial for the photocatalytic reactions. At the same time, more substrates are transported to catalytic active sites, thus the higher turnover number was obtained (Table 3).

After the reactions finished, the catalysts are separated by centrifugation, and the clear solutions are analyzed by UV–vis spectrophotometer and ICP-AES. There is no light absorption in the range from 190 to 300 nm for these solutions. In addition, detected concentration of W in these solutions is in the range from 1.1 to $3.3\,\mathrm{mg\,l^{-1}}$ (the initial concentration of W is in the

Fig. 9. Photodegradation of an aqueous MB ($0.065\,\mathrm{mmol\,l^{-1}}$, 100 ml) by UV-light irradiation of the different $H_3PW_{12}O_{40}/ZrO_2$ composites (0.1 g).

Table 3
Photocatalytic activity of $H_3PW_{12}O_{40}/ZrO_2$ in the photodegradation of aqueous 4-NP and MB[a]

Catalyst	TON for degradation of 4-NP[b]	TON for degradation of MB
5 TZ-773	14.6	1.5
10 TZ-773	9.5	1.5
15 TZ-773	6.9	1.3
20 TZ-773	4.1	1.4

[a] Initial concentration of 4-NP $0.36\,mmol\,l^{-1}$; initial concentration of MB $0.065\,mmol\,l^{-1}$; the system opened to air; the temperature of the suspension $30 \pm 2\,°C$; catalyst 0.1 g; UV light (50 W HPML) irradiation time 90 min.

[b] TON (turnover number) is based on mmol of 4-NP or MB consumed/mmol of active $H_3PW_{12}O_{40}$ site.

range from 36.7 to $110.2\,mg\,l^{-1}$), therefore, the leakage of the Keggin unit from the support is neglectable. The separated catalyst is used for another catalytic run, and the photoactivity is almost unchangeable for three times' run, suggesting that the strong interactions between the Keggin unit and ZrO_2 support ensure the little leaching of the Keggin unit from the support.

4. Conclusions

Novel solid Keggin-type POM, $H_3PW_{12}O_{40}/ZrO_2$ with different $H_3PW_{12}O_{40}$ loading levels and phase structures, are prepared by the modified wet impregnation method. The composites exhibit mesoporosity with average pore diameter in the range of 2.0–6.9 nm, and their BET surface area is higher than that of the starting $H_3PW_{12}O_{40}$ but lower than the corresponding ZrO_2 support. Impregnation of the Keggin unit into the ZrO_2 framework has an influence on the electronic properties of the ZrO_2, namely, the $H_3PW_{12}O_{40}/ZrO_2$ composites prepared by using the ZrO_2-623 (tetragonal phase) and ZrO_2-773 (the mixed phases of tetragonal and monoclinic) as the supports exhibit red shifted OMCT band, corresponding to relatively narrow bandgap.

Heterogeneous photocatalytic tests show that the increased photocatalytic activity compared with homogeneous $H_3PW_{12}O_{40}$ or ZrO_2 support is obtained with $H_3PW_{12}O_{40}$ loading levels not higher than 15 wt.%, mainly resulting from the increase the amount of photochemistry at longer wavelengths, phase structures, and surface physicochemical properties of the mesoporous materials.

Acknowledgments

References

[1] A. Molinari, R. Amadelli, L. Andreotti, A. Maldotti, J. Chem. Soc. Dalton Trans. (1999) 1203.
[2] R.R. Ozer, J.L. Ferry, Environ. Sci. Technol. 35 (2001) 3242.
[3] R.R. Ozer, J.L. Ferry, J. Phys. Chem. B 106 (2002) 4336.
[4] B. Yue, Y. Zhou, J. Xu, Z. Wu, X. Zhang, Y. Zou, S. Jin, Environ. Sci. Technol. 36 (2002) 1325.
[5] Y. Guo, C. Hu, X. Wang, E. Wang, Y. Zhou, S. Feng, Chem. Mater. 13 (2001) 4058.
[6] Y. Guo, C. Hu, S. Jiang, C. Guo, Y. Yang, E. Wang, Appl. Catal. B 36 (2002) 9.
[7] Y. Guo, C. Hu, C. Jiang, Y. Yang, S. Jiang, X. Li, E. Wang, J. Catal. 217 (2003) 141.
[8] L. Li, Q. Wu, Y. Guo, C. Hu, Micropor. Mesopor. Mater. 87 (2005) 1.
[9] Y. Yang, Q. Wu, Y. Guo, C. Hu, E. Wang, J. Mol. Catal. A 225 (2005) 203.
[10] Y. Yang, Y. Guo, C. Hu, Y. Wang, E. Wang, Appl. Catal. A 273 (2004) 201.
[11] D. Li, Y. Guo, C. Hu, L. Mao, Appl. Catal. A 235 (2002) 11.
[12] D. Li, Y. Guo, C. Hu, J. Mol. Catal. A 207 (2004) 181.
[13] D.A. Ward, E.I. Ko, Chem. Mater. 5 (1993) 956.
[14] H.H. Kung, Stud. Surf. Sci. Catal. 45 (1989) 721.
[15] A. Corma, Chem. Rev. 95 (1995) 559.
[16] J.-M. Herrman, J. Disdier, P. Pichat, J. Chem. Soc. Faraday Trans. 77 (1981) 67.
[17] J.A. Navío, G. Colón, Stud. Surf. Sci. Catal. 82 (1994) 325.
[18] A. Navío, M.C. Hidalgo, G. Colón, S.G. Botta, M.I. Litter, Langmuir 17 (2001) 202.
[19] K. Saito, M. Nomura, S. Ohgoshi, Y. Akai, Prep. Symp. Am. Chem. Soc. Div. Petro. Chem. 42 (1997) 712.
[20] E. López-Salinas, J.G. Hernández-Córtez, M. Cortéz, J. Navarrete, M. Yanos, A. Vázquez, H. Armdaris, T. López, Appl. Catal. 175 (1998) 43.
[21] Y. Izumi, K. Urabe, Chem. Lett. (1981) 663.
[22] M.A. Schwegler, H. Van Bekkum, N.A. De Munck, Appl. Catal. 74 (1991) 191.
[23] M. Valigi, D. Gazzoli, G. Ferraris, E. Bemporad, Phys. Chem. Chem. Phys. 21 (2003) 4974.
[24] J.B. Moffat, in: B. Imelik, et al. (Eds.), Catalysis by Acids and Bases, Elsevier, Amsterdam, 1985, p. 157.
[25] C. Rocchiccioli-Deltcheff, M. Fournier, R. Franck, R. Thouvenot, Inorg. Chem. 22 (1983) 207.
[26] E. López-Salinas, J.G. Hernández-Córtez, I. Schifter, E. Torres-Garc, T. López, Appl. Catal. A 193 (2000) 215;
J. Navarrete, A. Gutiérrez, T. López, P.P. Lottici, D. Bersani, Appl. Catal. A 193 (2000) 215.
[27] C. Wu, X. Zhao, Y. Ren, Y. Yue, W. Hua, Y. Cao, Y. Tang, Z. Gao, J. Mol. Catal. A 229 (2005), p. 229, 233.
[28] B.M. Devassy, S.B. Halligudi, S.G. Hegde, A.B. Halgeri, Chem. Commun. 10 (2002) 1074–1075.
[29] B.M. Devassy, F. Lefebvre, J. Catal. 231 (2005) 1.
[30] A.L. Linsebigler, G. Lu, J.T. Yates, Chem. Rev. 95 (1995) 735.
[31] A.A. Parks, Chem. Rev. 65 (1965) 177.